Triple Helix Formation and Homologous Strand Exchange in Pyrene-Labeled Oligonucleotides

S. Mohammadi,[‡] A. Slama-Schwok,*[,‡,§] G. Léger,[||] D. El Manouni,[||] A. Shchyolkina,[⊥] Y. Leroux,[||] and E. Taillandier[‡]

Laboratoire de Spectroscopie Biomoléculaire and Laboratoire de Chimie Structurale, URA CNRS 1430, UFR de Médecine et Biologie Humaine, Université Paris XIII, Bobigny, France, and Laboratory of Biopolymer Physics, Engelhardt Institute of Molecular Biology, Russian Academy of Sciences, Moscow, Russia

Received July 14, 1997; Revised Manuscript Received September 18, 1997[⊗]

ABSTRACT: The orientations of the symmetrical third strands ($G_3A_4G_3$) and ($G_3T_4G_3$) within the triplexes ($C_3T_4C_3$)−($G_3A_4G_3$)×($G_3A_4G_3$) and ($C_3T_4C_3$)−($G_3A_4G_3$)×($G_3T_4G_3$) were investigated by fluorescence spectroscopy and thermal denaturation using pyrene-labeled oligodeoxynucleotides. In the two triplex structures, both parallel and antiparallel orientations of the third strand with respects to the purine Watson−Crick one were identified by means of pyrene excimer formation. The pyrene labels do not modify the melting temperature of the ($C_3T_4C_3$)−($G_3A_4G_3$)×($G_3T_4G_3$) triplex but somewhat stabilize the corresponding duplex against thermal denaturation. The absorption melting profiles of the ($C_3T_4C_3$)−($G_3A_4G_3$)×($G_3A_4G_3$) triplex are monophasic in agreement with previous reports. In contrast, the melting of this structure, when monitored by the pyrene excimer band, reveals a biphasic behavior. These data, together with kinetics measurements, strongly suggest exchange mechanisms between the homologous oligomers ($G_3A_4G_3$), Hoogsteen, and Watson−Crick strands.

Oligonucleotide-directed triple-helix formation allows to design compounds with precise DNA sequence recognition (*1, 2*). The increasing interest in such structures arises from their potential application as antigene agents (*3*−*7*). Triplex formation requires a homopurine−homopyrimidine motif in the duplex targets. Pyrimidine Y, purine, and purine-rich R oligonucleotides can bind in the major groove of such duplexes with Y×Y−R or R×Y−R structural motifs. DNA triplex structures can be subdivided into three main classes according to the base composition of the Hoogsteen strand: CT, GT, and AG. While the first class usually requires a low pH to form the C^+×G−C triad, the other two classes exist at neutral pH (*8, 9*). In the latter classes, the orientation of the third strand with respects to the purine-rich Watson−Crick one is often considered as antiparallel with some exceptions (*3, 10*−*16*). Proper strand orientation is of particular importance in designing oligonucleotides capable of binding on the two strands of duplex DNA, that extend the range of triple helix application (*14, 17*−*19*).

The orientation of the third strand is usually determined by footprinting, affinity cleavage, sequence specific alkylation, or ligation (*1, 20*−*23*). NMR and X-ray data also provide information about the relative strand orientation (*24, 25*). The determination of the third strand orientation is not straightforward in the case of symmetrical sequences. In their paper directing the $A_3G_4A_3$ third strand to the $A_3G_4A_3$−$T_3C_4T_3$ duplex, Shafer and collaborators derived the strand orientation from gel-retardation assays by extrapolating from that obtained with an asymmetrical third strand $A_2G_2AGAG_3$ (*26*). The latter was found antiparallel to the purine Watson−Crick strand. The orientation of the $G_3T_4G_3$ third strand bound to the same target was investigated by introducing Malachite green at the 3′ end of the purine strand and rhodamine either at the 5′ or 3′ end of this G,T third strand (*27*). Although the two dyes strongly interact with each other and the efficiency of energy transfer is similar for the two orientations, it was deduced that the preferred orientation of the third strand is parallel to the purine strand of the duplex. Thus, nonperturbing and weakly interacting labels could be more adequate to determine triplex strand orientation. Pyrene-labeled oligonucleotides have been used by Jovin and co-workers to establish the existence of parallel-stranded duplexes, revealed by means of the pyrene excimer (*28*). When two pyrene molecules are in close proximity, the fluorescence spectrum exhibit a characteristic excimer band, red-shifted compared to the pyrene monomeric emission (*29*). The ratio of excimer to monomer intensity is often utilized as a measure of pyrene mobility and proximity (*30*). Typical distances of 4 Å between the pyrene molecules have been reported (*31*).

In the present work, the idea of Jovin and co-workers is extended to probe the strand orientation in triplex structures: two of the triplex strands are labeled with pyrene (see Chart 1). Only those orientation(s) in which the pyrene labels are in close proximity will display an excimeric emission. For that purpose, we use the $G_3A_4G_3$−C_3T_4 C_3 duplex with the homologous $G_3A_4G_3$ third strand as well as with the oligomer $G_3T_4G_3$ (*26, 32*−*37*). We were particularly interested by the GA strand since it gives rise to a peculiar all-or-none UV melting profile, in contrast with the GT strand that melts in an usual biphasic process (*36*). This also holds for other homologous GA oligomers (*15, 16, 38*−

* Corresponding author.
[‡] Laboratoire de Spectroscopie Biomoléculaire.
[§] Present adress: INSERM U310, Institut de Biologie Physico-Chimique, 13 Rue Pierre et Marie Curie, Paris, France. E-mail: schwok@ibpc.fr.
[||] Laboratoire de Chimie Structurale.
[⊥] Russian Academy of Sciences.
[⊗] Abstract published in *Advance ACS Abstracts,* November 15, 1997.

S0006-2960(97)01710-8 CCC: $14.00

Chart 1

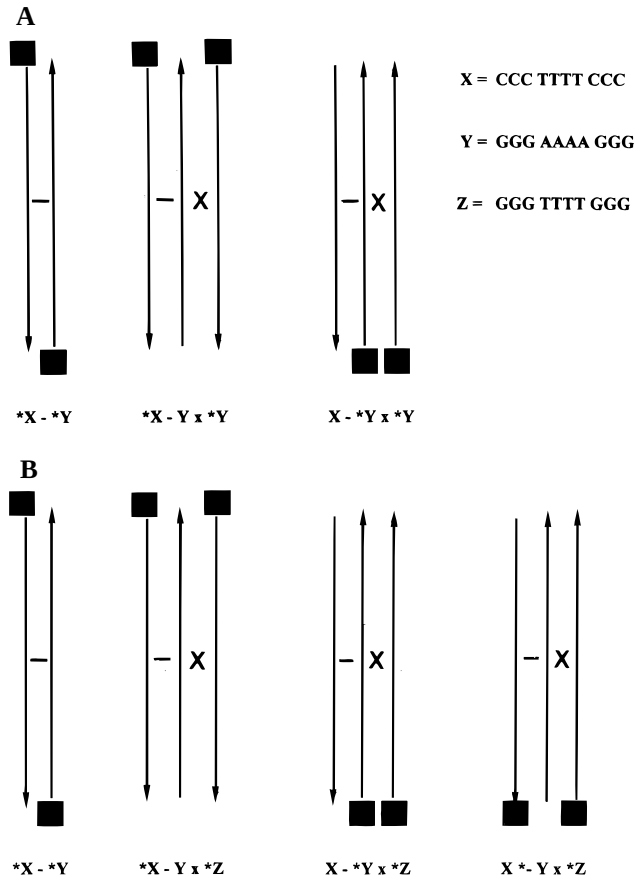

41). Our data, by means of pyrene excimer formation, reveals a strand exchange mechanism between the two homologous duplex and Hoogsteen GA strands. This process does not allow a total displacement of the third strand with increasing the temperature below the T_m of the duplex. We monitor the kinetics of these processes. These results may have implications in homologous recombination.

EXPERIMENTAL PROCEDURES

1. Materials. The succinimidyl-1-pyrenebutyrate (SPB) and phosphoramidites and the Aminolink 2 reagents were purchased from Molecular Probes and Applied Biosystems, respectively. Dioxane and dimethylformamide were Merck products. The chemicals used were of the highest commercial purity. The solutions contained 10 mM cacodylate buffer at pH = 7.2, 50 mM $MgCl_2$ unless otherwise stated. All aqueous solutions utilized Milli-Q water (Millipore).

2. Synthesis of the Oligonucleotides. The synthesis of the pyrene (Py)-labeled oligonucleotides was performed using a 391 Applied Biosystems Synthetizer as previously reported (*28*). The purity of the labeled oligomers was verified by an analytical chromatograph. Finally, the TEA^+ (triethanolamine counterions) oligomers were ion-exchanged on a Dowex resin to obtain Na^+ counterions. The sequences are 5′Py-CCCTTTTCCC3′, 5′CCCTTTTCCC-Py3′ , 5′Py-GGGAAAAGGG3′, and 5′Py-GGGTTTTGGG3′, called *X,X*, *Y, and *Z respectively.

3. Methods

3.1. Melting Temperatures. The T_m measurements were performed with a Kontron 941 spectrophotometer. The temperature of the cell holder was regulated by circulating water with a Neslab programmable cryothermostat, using temperature gradients of 12−15 °C/h. The temperature within the cell was measured with a temperature sensor. The melting profiles of the unlabeled oligonucleotides were monitored at 270, 259, and 257 nm and corrected for base line fluctuations by subtracting the absorbance at 350 nm. The melting of the duplex or triplex involving labeled oligomers was monitored at 347, 270, 259, and 257 nm and corrected with respects to the absorbance at 450 nm. The oligonucleotides samples used for melting experiments were slowly heated to 70 °C for 30 min then gently cooled to 5 °C and maintained at this temperature overnight for equilibration before measurements**.** In the case of triplex formation, the third strand, previously heated to 70 °C, was added to the preformed duplex at 5 °C; this procedure was found to reduce the self-association(s) of the third strand and favor triplex formation (*26*). The self-association of the Y strand can be readily detected by the appearance of an excimer, especially if the solution was not previously heated (Figure 5A and data not shown).

3.2. Fluorescence Measurements. The fluorescence measurements were performed with a Fluoromax instrument (Spex) equipped with a Hamamatsu 928 photomultiplier (PM) and a thermostated cell holder. The data have been corrected for the PM response and lamp fluctuation and for the variation of the absorption at the exciting wavelength. Repeated fluorescence spectra of the labeled oligomers induce a decrease of the fluorescence intensity under continuous 349 nm irradiation. This was reduced by taking short integration times and small excitation path lengths, l = 0.4 cm, and small excitation and emission slits (1.2 nm). The area under the fluorescence curves were calculated to obtain the relative fluorescence quantum yield of the different structures using anthracene and pyrene as references at 20 °C (*42*).

RESULTS

1. Spectroscopic Features of X, Y, and Z Strands and of the X−Y Duplex

*1.1. Absorption and Fluorescence Yields of *X, *Y, and *Z Alone.* Pyrene labels are attached to CCCTTTTCCC, named *X or X*, according to the label linked at the 5′ or 3′ end, respectively, GGGAAAAGGG, *Y, and GGGTTTTGGG, *Z. The pyrene band of these labeled oligomers is a red-shifted compared to pyrene in ethanol, λ_{max} = 334 nm (Table 1). This effect has been previously reported for pyrene conjugated to polynucleotide and tRNA (*43*). The pyrene fluorescence maxima are affected by the covalent attachment to the DNA oligomers, and the fine vibronic structure of pyrene in ethanolic solutions is lost (*44*). The excitation maxima generally correspond to the absorption peaks of the pyrene.

The fluorescence yields strongly vary upon the sequence of the DNA fragment, as shown in Table 1. Both *Y and *Z strands have a high yield, but the fluorescence of the *X oligomer is strongly quenched. The attachment of the pyrene at the 3′ end of the same symmetrical sequence, X*, yields a higher fluorescence yield than that of *X. Quenching of pyrene fluorescence has been observed by CMP, UMP, and when covalently attached to nucleic acids depending on the sequence (*45*−*47*).

Table 1: Spectroscopic Properties of the Unlabeled and Pyrene-Tagged Oligonucleotides

	λ_{max}					T_m	
sequence	abs Py (nm)	exc (nm)	[excimer]/[monomer][a]	Φ/Φ[b]	Φ[c]	abs (±1 °C)[d]	fluo (±2 °C)[d]
*X	347	341	*n*	1.0	2.8×10^{-3}		
X*	347	342	*n*	6.0	2.1×10^{-2}		
*Y	348	347	0.04	60	0.33		10, 25
*Z	349	348	*n*	37	0.13		20, 42
X−Y						47	
*X−Y	348	345	*n*	0.7		52	51
X−*Y	347	346	*n*	2.4		51	
*X−*Y	347	346	*n*	1.5		58	57
X*−Y	347	342	*n*	1.5		52	
X−Y×Y						47	
*X−Y×*Y	347	347	0.27	12.5		57	32, 58
X−*Y×*Y	347	348	0.09	10.0		52	25, 52
X−Y×Z						23, 48	
*X−Y×*Z	348	348	0.12	12.5		22, 50	23, 55
X−*Y×*Z	347	348	*n*	10.0			
X*−Y×*Z	347	348	0.06	14.8			15, −

[a] Ratio of the intensity at excimer maximum relative to that at 378 nm, measured at 5 °C, the error on the ratio is ± 0.015; *n* stands for a ratio smaller than the error, abs for absorption, exc for excitation, and fluo for fluorescence. [b] Fluorescence yield relative to that of *X measured at 5 °C [c] Fluorescence yield measured relative to quantum yield standards at 20 °C (see Experimental Procedures). [d] The T_m are determined by the first derivative of absorption (abs) and fluorescence (fluo) profiles, using 20 μM (in phosphate units) of each strand.

When the fluorescence spectrum of the *Y oligomer is measured at 5 °C, a weak excimeric emission is observed. This sequence that contains two runs of 3 consecutive guanines spaced by 4 adenines is often self-associated (*15*, *16*, *28*, *48*). The Z strand alone may form quadruplex structures (asymmetric hairpin dimer) under proper experimental conditions (*34*, *37*, *49*−*50*). *Z does not present an excimeric emission.

1.2. Comparison of the Absorption and Fluorescence Melting Curves of the Duplex. Pyrene labeling increases the (absorption) melting temperature of either *X−Y, X*−Y, or X−*Y duplexes found at 52 ± 1 °C compared to the T_m of X− Y, observed at 47 ± 1 °C. The T_m of the *X−*Y duplex occurs at 58 ± 1 °C. Table 1 shows that the quantum yield of the duplex is much lower than that of the *Y strand. Thus, melting curves are easily obtained by monitoring the fluorescence of the pyrene which intensity increases with the temperature (Figure 1A). A typical fluorescence melting profile is shown in Figure 1B for the *X−*Y duplex, similar to that obtained by absorption.

2. Fluorescence Characterization of the X−Y×Y Triplex

2.1. Strand Orientation. The formation of the X−Y×Y triplex has been previously reported (*36*). This structure contains homologous and symmetrical oligomers as Watson−Crick purine and third strands. Alternative pyrene labeling allows a straightforward insight of the strand orientation. Figure 2 compares the normalized fluorescence spectra of the *X−*Y duplex to that of the X−*Y×*Y and *X−Y×*Y structures (curves a, b, and c respectively). The lack of any excimer in curve a is expected from the antiparallel orientation of the Watson−Crick strands in the *X−*Y duplex, Chart 1. The broad excimeric emission of pyrene (curve c) is obvious for the *X−Y×*Y triplex. The excitation spectra recorded at λ_{em} = 378 and 490 nm are identical, in agreement with the excimeric nature of the low-energy emitting band. The presence of this excimer reveals an antiparallel orientation of the two Y strands of the *X−Y×*Y triplex.

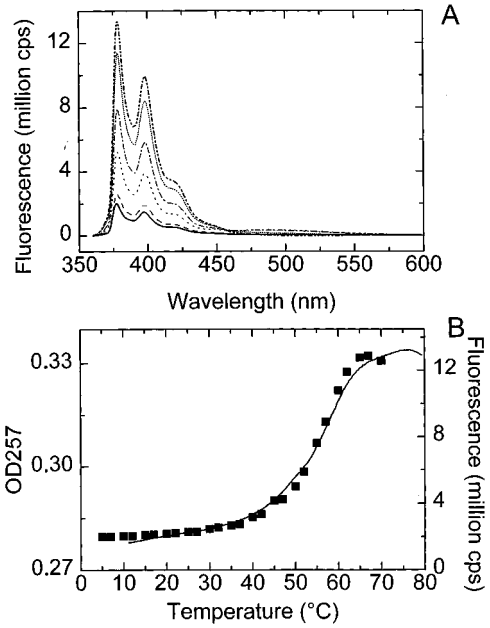

FIGURE 1: (A) Temperature dependence of the fluorescence spectra of the *X−*Y duplex. The solutions are prepared in 10 mM cacodylate buffer at pH = 7.2 containing 50 mM $MgCl_2$. The strand concentration is [*X] = [*Y] = 20 μM in phosphate units. The exciting wavelength is λ_{exc} = 349 nm, and the slits are 1.2 nm. From bottom to top: (—) 5 °C; (− −) 32 °C; (---) 50 °C; (−· −) 55 °C; (···) 60 °C; and (− ·· −) 65 °C. (B) Comparison of the melting profile of *X−*Y by absorption and fluorescence. Same solution conditions as in A. Full line and left scale, melting curve monitored at 257 nm; full squares and right scale, melting profile detected at λ_{exc} = 349 nm and λ_{em} = 378 nm.

The X−*Y×*Y triplex gives rise to a weak excimer shown in curve b, suggesting the existence parallel-oriented conformers. The Y strand alone at this temperature exhibits a weaker excimeric emission than the triplex. This difference will be confirmed by the comparison of the two melting curves (section 2.4 and Figure 5). It is however difficult to quantify the relative proportion of the two triplexes. Although their monomer yield is similar, the excimer fluorescence yield of the parallel and antiparallel structures could

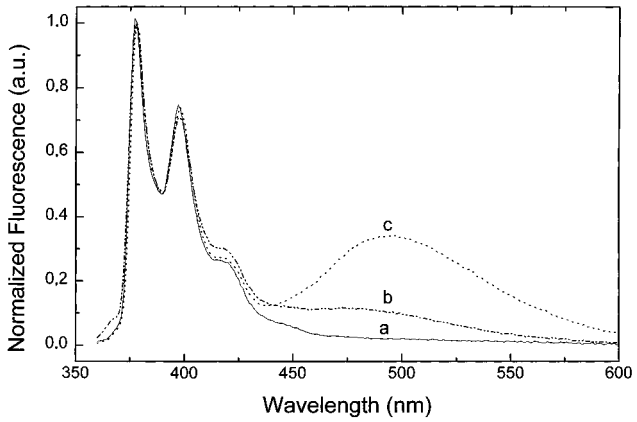

FIGURE 2: Comparison of the normalized fluorescence spectra of the *X−*Y duplex and the X−*Y×*Y and *X−Y×*Y triplexes. the curves are noted as a, b, and c respectively. All strand concentrations are 20 μM in phosphate units. The spectra are measured at 5 °C. The exciting wavelength is λ_{exc} = 349 nm, and the slits are 1.2 nm.

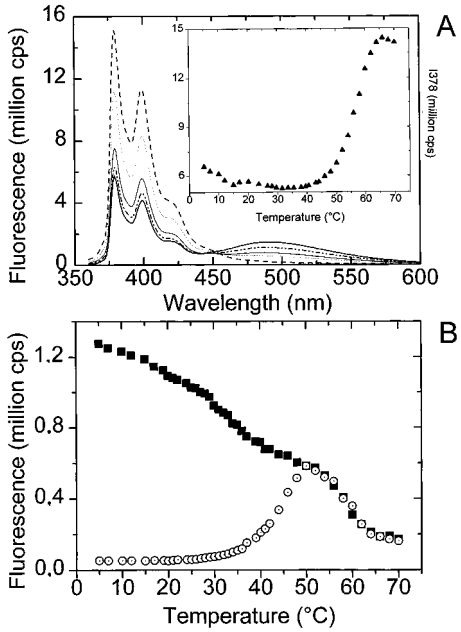

FIGURE 3: (A) Temperature dependence of the fluorescence spectra of the *X−Y×*Y triplex. Same conditions as in Figure 1; from bottom to top: (—) 5 °C, (---) 25 °C; (— ·· —) 35 °C; (—) 50 °C; (···) 57 °C; and (— —) 70 °C; insert, fluorescence intensity of *X−Y×*Y followed at 378 nm as a function of the temperature. (B) Melting profile of the *X−Y×*Y triplex. Same conditions as in Figure 1, λ_{exc} = 349 nm: squares, fluorescence intensity of the triplex monitored at 490 nm; circles, fluorescence intensity of the *X−*Y duplex detected at the same wavelength;.

be different because of the different environments of the labels within the two structures.

*2.2. Melting Curves of the *X−Y×*Y Triplex.* The spectral changes induced by heating the *X−Y×*Y triplex are presented in Figure 3. The temperature increase from 5 to 35 °C results in a intensity decrease of the excimer band while the monomeric emission is slightly enhanced. Further heating to 70 °C induces the disappearance of the excimer and a large increase of the 378 nm peak. One can note the presence of an isoemissive point at 438 nm observed between 5 and 50 °C, replaced by another one at 452 nm obtained above 50 °C.

The plot of the intensity at 378 nm as a function of the temperature (Figure 3A insert) gives a similar melting temperature at T_m = 58 ± 1 °C as for the *X−*Y duplex (Figure 1B). The *X−Y×*Y melting curve monitored at 494 nm is shown in Figure 3B. This melting profile exhibits two main transitions, the first one occurring around 32 °C, the second one at 58 °C. The fluorescence and absorption melting curve are fully reversible.

A recent publication has shown that this (unlabeled) triplex melts in a monophasic transition by a variety of techniques; the authors have attributed this behavior to the triplex dissociation in an all-or-none fashion (*36*). In the present case of the labeled pyrene oligomers, the absorption melting curves give a single monophasic transition at the same T_m as the duplex (Table 1), following the same trend as the unlabeled triplex. These data rise questions about the mechanism of the melting of the *X−Y×*Y triplex. Several hypothesis can be made to account for our data, that are not necessarily mutually exclusive. The first one assumes that the pyrene labeling destabilizes the tagged triplex compared to the unlabeled one. Alternatively, the first melting transition could correspond to an incomplete removal of the *Y third strand until completion of the duplex melting. The triplex melting has to be partial to account for the excimeric emission still left above the first transition. Another related hypothesis relies on the exchange between the homologous Y strands. This exchange should begin when some of Y third strand is released (equilibrium 1) and is expected to end at about 65 °C at melting completion. The third strand may be partly maintained above the melting point at 32 °C because of competing equilibria: a strand exchange between the unlabeled Y duplex and the labeled one, occurring at the duplex level (eq 2) and a triplex rearrangement via equilibrium 3.

$$*X-Y\times*Y \rightleftharpoons *X-Y + *Y \quad (1)$$

$$*X-Y + *Y \rightleftharpoons *X-*Y + Y \quad (2)$$

$$*X-Y\times*Y \rightleftharpoons *X-*Y\times Y \quad (3)$$

Some evidence supporting a partial third strand release mechanism(s) is provided by the *X−*Y melting curve. One can notice, from Figures 1A and 3B, the existence of a weak excimeric emission that is absent at 5 °C but induced by heating the duplex above ~30 °C. This excimer can only be explained by the formation of some *X−*Y×*Y triplex via an equilibrium similar to eq 1, in competition with *X−*Y duplex melting. As the temperature is increased, melting of the duplex is favored over triplex formation and the excimer intensity decreases. This decrease, observed above ~52 °C, overlaps within experimental error with the melting curve of *X−Y×*Y triplex (Figure 3B). Further supports of the proposed exchange mechanism(s) are given below by following the kinetics of excimer formation at 5 °C.

*2.3. Kinetics of Triplex Formation and Strand Exchange in *X−Y×*Y.* The data of Figures 1 and 2 indicate that, at 5 °C, *X−*Y does not form an excimer, in agreement with the antiparallel orientation of its strands, the low temperature insuring that all *Y is engaged in the duplex. If we now add increasing concentrations of the unlabeled Y strand, the formation of an excimer can only be explained by a (or several) mechanism(s) involving strand exchange such as those proposed in equations 1−3. Figure 4A presents the time course of the spectral modification of a solution

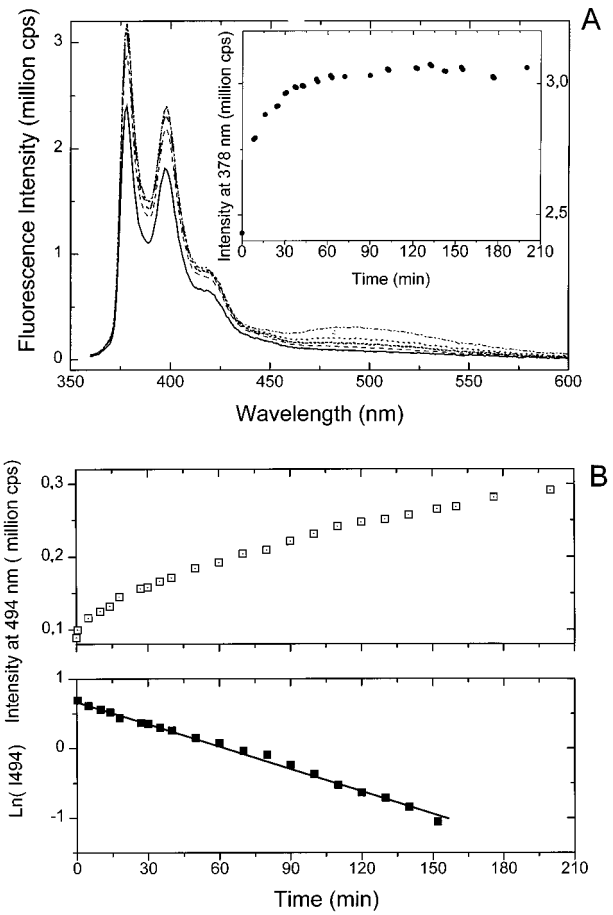

FIGURE 4: (A) Time course of the excimer formation at $T = 5$ °C. At time $t = 0$, the solutions contains [*X] = [*Y] = 20 μM and [Y] = 4 μM in 10 mM cacodylate buffer at pH = 7.2 and 50 mM $MgCl_2$. The fluorescence spectrum of this solution is represented as a full (bottom) line (—). An aliquot of a concentrated Y solution is added such that the total Y concentration becomes [Y] = 8 μM. The fluorescence spectra are recorded as a function of time at t = 6 min (– –); t = 23 min (---); t = 55 min (···); and t = 180 min (– ·· –). (Insert) Time profile of the reaction followed at 378 nm. (B) Time profile of the excimer formation at 5 °C. Same conditions as in A; the reaction is followed at 494 nm in the upper part (squares) and in the lower part plot of the logarithm of the (final fluorescence minus that observed at time t) at 494 nm versus time.

Table 2: Half-Time Values of the Spectroscopic Changes Occurring after Mixing the Labeled Duplex with Untagged Third Strand

[Y]/[*X−*Y]		*I*494/*I*378	$t_{1/2}$ at 378 nm (min)	$t_{1/2}$ at 494 nm (min)
$t = 0$	$t = \infty$	at $t = \infty$	monomeric emission	excimeric emission
0	0.2	0.037	(4 ± 1)	(35 ± 5)
0.2	0.4	0.103	(8 ± 1)	(63 ± 7)
0.4	1.0	0.300	(18 ± 2)	>180

containing 1 equivalent of *X−*Y and 0.2Y to which another 0.2 equivalent of Y is added at time $t = 0$. A fast increase of the 378 nm peak is observed within 30 min (Figure 4A, insert). An excimeric band is formed at a slower rate (Figure 4B). The kinetics could not be determined more accurately since some degradation of the pyrene labels occur after (about 50) repetitive scans. The first half-time of the processes, $t_{1/2}$, differs when the process is monitored at 378 from that at 494 nm (Table 2). Two-step kinetics are also observed at different ratio of [*X−*Y] over [Y]. The excimeric emission increase mainly follows a first-order rate law (Figure 4B).

Scheme 1: Proposed Mechanism of the Antiparallel Triplex (Excimer) Formation[a]

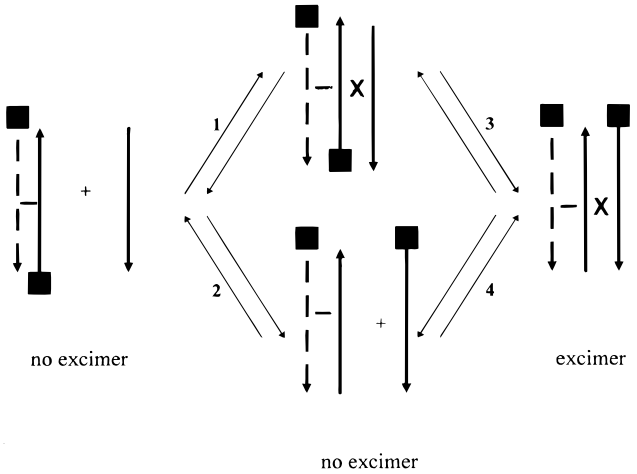

[a] The X strand, ($C_3T_4C_3$), is represented as a dashed arrow, the Y strand ($G_3A_4G_3$), as a full arrow. Exchange between the homologous Y strands may occur via the duplex and/or the triplex, equilibria 2 and 3, respectively.

The possible mechanisms, that can account for the data, are depicted in Scheme 1. The initial increase at 378 nm should result from the triplex formation, reaction 1, since the triplex yield is higher than that of the duplex (Table 1). However, a strand exchange equilibrium 2 may compete with triplex formation 1. This process could be favored at low [Y] over [*X−*Y] ratios, accounting for the much smaller excimer at 0.2[Y] relative to that observed at 1[Y] (Table 2). Both pathways yield non-excimeric intermediates, either *X−*Y×Y or *X−Y + *Y, which both could result in the excimeric *X−Y×*Y triplex. This triplex can be formed either via triplex strand exchange 3 and/ or via reaction 4.

The kinetics of the excimer formation is essentially first order, consistent with equilibrium 3, a triple-helix-mediated strand exchange. The $t_{1/2}$ dependence in Y concentration suggests a contribution of equilibrium 2. These results are consistent with the above hypothesis of strand exchange between homologous Watson−Crick and third strands (section 2.2).

*2.4. Melting Curve of the X−*Y×*Y Triplex.* The spectroscopic changes induced by heating the X−*Y×*Y triplex are presented in Figure 5. The melting monitored at 378 nm results in a T_m value of 52 ± 1 °C, the same as that of the corresponding X−*Y duplex (Table 1). The fluorescence intensity of the melted triplex at 70 °C is about twice that of the *Y strand alone as expected from the presence of two *Y strands in this triplex (Figure 5B). The temperature dependence of the triplex excimer is compared to that of the *Y strand in Figure 5A. The self-associated *Y strands melt at $T_m = 10$ °C, the presence of the Y excimer indicating a parallel-stranded structure. In contrast, the triplex excimer presents the first melting transition around 25 °C. This melting is associated with the existence of an isoemissive point at 433 nm between 5 and 32 °C, lost upon further heating. Above this first transition, the excimer intensity does not drop to zero, as in the case of the *X−Y×*Y triplex. The first transition is reversible in the time scale of days, only if the temperature is not increased more than 40 °C. This slow reversibility implies that the T_m value observed for this triplex is an apparent one; it differs from that observed with the *X−Y×*Y triplex.

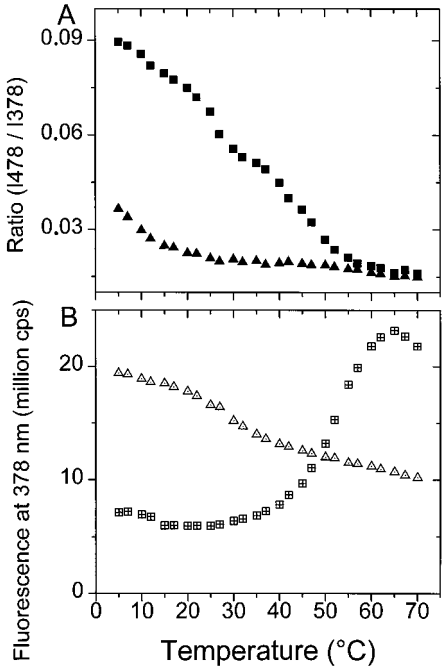

FIGURE 5: Melting profiles of the X−*Y×*Y triplex compared to that of the *Y strand alone. The triplex is represented as squares whereas the *Y strand is noted as triangles. The triplex solution contains [X] = 20 and [*Y] = 40 μM whereas *Y alone concentration is 20 μM in 10 mM cacodylate buffer at pH = 7.2 containing 50 mM $MgCl_2$. (A) Ratio of the fluorescence intensities followed at 478 nm (I478) over that at 378 nm (I378). (B) Fluorescence intensity monitored at 378 nm.

3. Fluorescence Characterization of the X−Y×Z Triplex

3.1. Strand Orientation. The X−Y duplex also forms a triplex structure with the third strand Z. The melting of this structure has been recently reported and the third strand was proposed to be parallel with respects to the purine Watson−Crick strand (*27*, *36*). However, since the Z oligomer contains G and T bases, the orientation of this strand depends on the target homopurine sequence according to the number, the size and the position of GpT and TpG steps (*11*, *14*). Molecular modeling predicts an antiparallel orientation if there are more than three such steps and a parallel orientation if there is only one ApG step. The present experiment with pyrene labeled strands allows to determine the orientation of the *Z strand (Chart 1B) as shown in Figure 6. The fluorescence of the two triplexes *X−Y×*Z and X−*Y×*Z differ markedly by the presence of an excimeric emission for the former, absent in the latter. However, the absence of an excimeric emission in X−*Y−*Z does not necessary imply that the parallel-oriented triplex does not exist. The effect may originate from a particularly low fluorescence yield of X−*Y−*Z excimer. To check this possibility, the strand orientation is also tested with a label attached at the 3′ end of the X strand, called X*. Figure 6 (insert) shows that X*−Y×*Z presents a weak excimeric emission with this alternative labeling. This weak excimer reveals that some of the triplex species are oriented in a parallel manner with respects to the purine Y strand. It seems probable that the fluorescence yield of the X−*Y−*Z excimer differs from that of X*−Y×*Z one, since both structures have the parallel strand orientation. Table 1 shows similar qualitative differences at the duplex and X strand level. Differences between 5′ and 3′ pyrene end labeling have been reported (*47*).

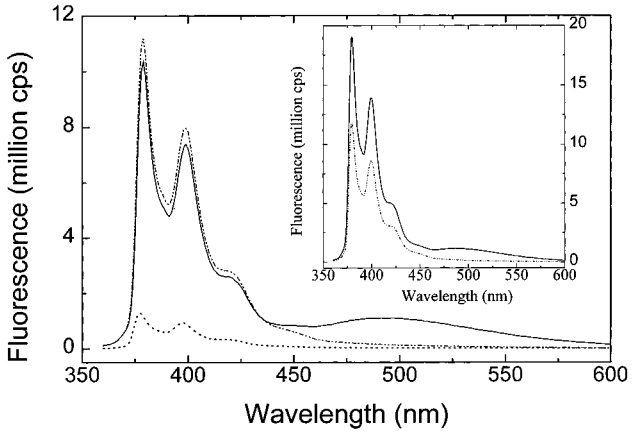

FIGURE 6: Comparison of the fluorescence spectra of the X−*Y duplex and the X−*Y×*Z and *X−Y×*Z triplexes. All strand concentrations are 20 μM in phosphate units. The spectra are measured at 5 °C. The exciting wavelength is λ_{exc} = 349 nm, and the slits are 1.2 nm. X−*Y (···); *X−Y×*Z (—); and X−*Y×*Z (− ·· −); Insert: comparison of the spectra of the X−*Y×*Z and X*−Y×*Z triplexes, (− ·· −) and (—) respectively.

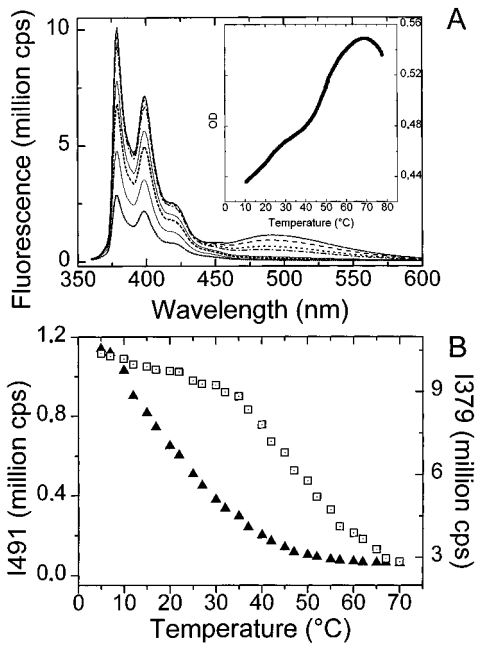

FIGURE 7: (A) Temperature dependence of the fluorescence spectra of the *X−Y×*Z triplex. Same conditions as in Figure 6; from top to bottom T = 5 °C (—); 12 °C (− −); 20 °C (---); 25 °C (− · −), 40 °C (—); 45 °C (---); 55 °C (—) and 70 °C (···); insert, melting curve of the triplex followed by absorption at 259 nm. (B) Melting profiles of the *X−Y×*Z triplex. Same conditions as in Figure 6: left scale and triangles, fluorescence monitored at 491 nm; right scale and squares, fluorescence intensity recorded at 379 nm.

The data enables to attribute the orientations of the Z strand as both parallel and antiparallel to the homopurine Y strand. These results could be expected on the basis of molecular modeling: two (G/T) steps seem sufficient to promote some antiparallel orientation but not enough to destabilize completely the parallel one.

*3.2. Melting Curves of the *X−Y×*Z Triplex.* The melting profile of the *X−Y×*Z triplex is then monitored by fluorescence and absorption spectroscopy. Figure 7 shows that increasing the temperature results in a decrease of both monomeric and excimeric emissions. The melting recorded in the excimer band is observed at T_m = 22 ± 1

°C in agreement with the first transition monitored by absorption. The decrease of the monomeric band at 379 nm with the temperature is consistent with the second transition also detected by absorption at $T_m = 51 \pm 1$ °C. This last value corresponds to the melting temperature of the *X−Y duplex (Table 1). The data therefore point out at a two-step melting profile, the first one corresponding to the disruption of the triplex structure, the second one monitoring the duplex melting, in agreement with previous reports (*36*).

DISCUSSION

1. X−Y×Y Triplex

The formation of the X−Y×Y triplex has been previously reported (*26*, *36*). This structure contains homologous Y oligomers as Watson−Crick and third strands. Alternative labeling of the duplex strands in the presence of an 5′ tagged *Y third strand enables to identify an excimeric emission in both parallel and antiparallel third strand orientation although the fluorescence yield of the former is much lower than that of the latter.

In contrast with the melting curves obtained by absorption, the fluorescence melting profiles of the excimers present two transitions (Figures 3B and 5A). Heating above the lower transition does not abolish the excimeric emission, as expected from the release of the triplex third strand. This suggests that this strand is not completely dissociated from the duplex, pointing out at one or several equilibria, which partly maintain the third strand association. The excimer drops to essentially zero only once the duplex is dissociated. We have examined the possibility of strand exchange between the identical Y sequences, the purine and third strands, as part of a possible explanation accounting for these data. When an unlabeled Y strand is added to the preformed *X−*Y duplex, we first observe an increase of the monomer fluorescence intensity followed by the formation of the excimer at a slower rate. Although degradation of the labels under continuous irradiation do not allow a fit of the data according to the proposed Scheme 1, we may reach the below qualitative conclusions:

(i) The formation of the excimer from *X−*Y duplex and unlabeled Y implies the occurrence of the *X−Y×*Y triplex. This structure can only form by mechanism(s) involving strand exchange. This process takes place in the hour(s) time scale and obeys to first-order kinetics. This is expected from a rearrangement reaction such as triplex-mediated strand exchange (equilibrium 3).

(ii) The initial increase of fluorescence at 378 nm is attributed to the triplex *X−*Y×Y formation via equilibrium 1, since the triplex yield is much higher than that of the duplex (Table 1). This process is completed faster than the excimer buildup. However, the $t_{1/2}$ measured at this wavelength may include the contribution of a competing reaction 2 describing a strand exchange at the duplex level. Such a reaction probably lowers the occurrence of triplex formation. In fact, Scheme 1 is probably simplified, since it does not describe the possibility of a change in strand orientation, antiparallel to parallel, that may also occur. Due to the complexity of the scheme and the experimental difficulties, our $t_{1/2}$ values cannot be compared directly with the literature (*35*, *51*−*54*).

(iii) The proposed strand exchange via triplex rearrangement is expected to depend very strongly on the identity of the purine and third strands and also on their length. One may suggest that this exchange will become slower upon increasing the two strands length. This hypothesis may explain the effect of third strand length reported by Malvy and co-workers (*38*, *39*). These authors used a 20-mer duplex target together with (G,A) strand which size varied from 11 to 20 nucleotides. The melting profiles were always monophasic but in the case of the 20-mer, the heating profile was "rate-dependent". These authors suggested that, "before the melting, the triplex structure passes over an energetic barrier or undergoes a slow rearrangement step" (*38*). They also found that a single mismatch abolishes triplex formation, that could be compatible with our proposed scheme. The strand homology is a strong requisite for this triplex formation.

The strand exchange has been tested for the antiparallel triplex *X−Y×*Y. We assume that the parallel X−*Y×*Y triplex could also undergo similar mechanisms, based on the biphasic decrease of the excimer with increasing the temperature, similar to that observed for the antiparallel triplex. The reversibility of the melting curves of the parallel and antiparallel triplexes differ: the former is complete within the experiment time, independently on the initial and final temperatures whereas the latter requires that heating does not overcome the 40 °C temperature range. Since this temperature coincides with the beginning of duplex melting, this hints at a peculiar duplex structure within X−*Y×*Y triplex, that cannot be recovered after complete strand dissociation. This contrasts with the behavior of the antiparallel triplex, suggesting that the duplex structure within the X−*Y×*Y and *X−Y×*Y triplexes are not identical. A molecular modeling study has reported the structures of parallel and antiparallel triplexes with a purine-rich third strand containing either GpA or ApG steps, occurring in our Y strand (*55*). For the antiparallel triplex, the equilibrium state is soon reached. In contrast, the parallel triplex requires a slow and progressive reorganization of the phosphodiester chain within the Watson−Crick duplex. These observations may be relevant to our present data. The lower (apparent) T_m value of the parallel-stranded triplex suggests a lower stability of the latter relative to the antiparallel structure.

(iv) Our results suggest that strand exchange between short oligomers may occur in vitro in homologous sequences and probably takes place in both parallel and antiparallel orientations. The presence of the RecA protein (*56*−*60*) in the solution should discriminate between the two orientations and catalyzes specifically the antiparallel one.

2. X−Y×Z Triplex

The use of pyrene labels enables to attribute the orientations of the Z strand as both parallel and antiparallel to the homopurine Y strand in the X*−Y×*Z and *X−Y×*Z triplexes, respectively. These orientations have been observed by Shafer using energy transfer measurements using labeled Y and Z strands (*27*). However, these authors conclude that the parallel orientation is preferred because of its higher thermal stability relative to the antiparallel triplex. In both orientations, the triplex melting temperatures are substantially increased compared to the unlabeled one. This effect arises from strong dye to dye interaction, assumed similar by these authors in both orientations. In our case of pyrene-labeled X−Y×Z triplexes, the melting temperature

of the third strand removal is identical within experimental error whether labeled or unlabeled oligomers are used, showing that pyrene−pyrene interactions are not perturbing the triplex. The melting temperature of the antiparallel triplex is 22 °C, whereas that of the parallel one is about 15 °C, although the value could not be determined with great precision because of the low yield of the corresponding excimer. The related absorption derivative profile shows a main peak at 23 °C, together with a shoulder, centered around 17 °C. This may suggest that the two parallel and antiparallel oriented triplexes do not differ much in terms of their thermal stability. The existence of the two orientations could be expected on the basis of molecular modeling: two (G/T) steps seem sufficient to promote some antiparallel orientation but not enough to destabilize completely the parallel one (*11*).

CONCLUSION

($G_3A_4G_3$) forms two triplex structures with the ($C_3T_4C_3$)−($G_3A_4G_3$) duplex, accounting for the pyrene excimer found with alternative strand labeling: the third strand can be parallel and antiparallel to its homologous Watson−Crick strand, but the fluorescence of the former excimer is much lower than that of the latter. In contrast with the monophasic absorption melting profile, the intensity of the excimer band, in both parallel and antiparallel structures, decreases in a biphasic manner upon increasing the temperature. These data, together with the kinetics of the *****($C_3T_4C_3$)−($G_3A_4G_3$)×*****($G_3A_4G_3$) triplex formation from preformed *****($C_3T_4C_3$)−*****($G_3A_4G_3$) duplex with unlabeled ($G_3A_4G_3$), strongly suggest strand exchange mechanisms between the homologous ($G_3A_4G_3$) strands.

The ($G_3T_4G_3$) oligomer also forms parallel and antiparallel triplex structures with the ($C_3T_4C_3$)−($G_3A_4G_3$) duplex, in agreement with previous molecular modeling reports. The fluorescence yield of the excimer is dependent on the position of the pyrene label, at 5′ or 3′ end. The melting temperatures of these triplex structures, monitored by absorption and fluorescence, do not differ much from their unlabeled counterpart, suggesting that pyrene labeling does not significantly disturb the triplex.

REFERENCES

1. Moser, H. E., and Dervan, P. B. (1987) *Science 238*, 645−650.
2. Le Doan, T., Perouault, L., Chassignol, M., Thuong, N. T., and Hélène, C. (1987) *Nucleic Acids Res. 15*, 8643−8659.
3. Durland, R. H., Kessler, D. J., Gunnel, S., Duvic, M., Pettit, B. M., and Hogan, M. E. (1991) *Biochemistry 30*, 9246−9255.
4. McShan, W. M., Rossen, R. D., Laughter, A. H., Trial, J. A., Kessler, D. J., Zendegui, J. G., Hogan, M. E., and Orson, F. M. (1992) *J. Biol. Chem. 267*, 5712−5721.
5. Giovannangeli, C., Thuong, N. T., and Hélène, C. (1992) *Nucleic Acids Res. 20*, 4275−4281.
6. Thuong, N. T., and Hélène, C. (1993) *Angew. Chem., Int. Ed. Engl. 32*, 666−690.
7. Alunni-Fabbroni, M., Manfioletti, G., Manzini, G., and Xodo, L. E. (1994) *Eur. J. Biochem. 226*, 831−839.
8. Plum, G. E., Pilch, D. S., Singleton, S. F., and Breslauer, K. (1995) *Annu. Rev. Biophys. Biomol. Struct. 24*, 319−350.
9. Roberts, R. W., and Crothers, D. M. (1996) *Proc. Natl. Acad. Sci. U.S.A. 93*, 4320−4325.
10. Beal, P. A., and Dervan, P. B. (1991) *Science 251*, 1360−1363.
11. Sun, J.-S., De Bizemont, T., Duval-Valentin, G., Montenay-Garestier, T., and Hélène, C. (1991) *C.R. Acad. Sci. Paris 313*, 585−590.
12. Mayfield, C., Squibb, M., and Miller, D. (1994) *Biochemistry 33*, 3358−3363.
13. Svinarchuk, F., Bertrand, J.-R., and Malvy, C. (1994) *Nucleic Acids Res. 22*, 3742−3747.
14. De Bizemont, T., Duval-Valentin, G., Sun, J.-S., Bisagni, E., Garestier, T., and Hélène, C. (1996) *Nucleic Acids Res. 24*, 1136−1143.
15. Alunni-Fabbroni, M., Pirulli, D., Manzini, G., and Xodo, L. E. (1996) *Biochemistry 35*, 16361−16369.
16. Alunni-Fabbroni, M., Manzini, G., Quadrifolio, F., and Xodo, L. E. (1996) *Eur. J. Biochem. 238*, 143−151.
17. Beal, P. A., and Dervan, P. B. (1992) *J. Am. Chem. Soc. 114*, 4976−4982.
18. Froehler, B. C., Terhorst, T., Shaw, J. P., and McCurdy, S. N. (1992) *Biochemistry 31*, 1603−1609.
19. Jayasena, S. D., and Johnston, B. H. (1993) *Biochemistry 32*, 2800−2807.
20. Strobel, S. A., Doucette-Stamm, L. A., Riba, L., Housman, D. E., and Dervan, P. B. (1991) *Science 254*, 1639−1642.
21. Luebke K. J., and Dervan, P. B. (1991) *J. Am. Chem. Soc. 113*, 7447−7448.
22. Povsic, T. J., and Dervan, P. B. (1992) *J. Am. Chem. Soc. 114*, 5934−5941.
23. Grant, K. B., and Dervan, P. B. (1996) *Biochemistry 35*, 12313−12319.
24. Rajagopal, P., and Feigon, J. (1989) *Nature 339*, 637−640.
25. van Meervalt, L., Villeghe, D., Dautant, A., Gallois, B., Précigoux, and G. Kennard, O. (1995) *Nature 374*, 742−744.
26. Pilch, D. S., Levenson, C., and Shafer, R. H. (1991) *Biochemistry 30*, 6081−6087.
27. Scaria, P. V., Wills, S., Levenson, C., and Shafer, R. H. (1995) *J. Biol. Chem. 270*, 7295−7303.
28. Rippe, K., Fritsch, V., Westhof, E., and Jovin, T. M. (1992) *EMBO J. 11*, 3777−3786.
29. Ebata, K., Masuko, M., Ohtani, H., and Kashiwasake-Jibu, M. (1995) *Photochem. Photobiol. 62*, 836−839.
30. Lochmüller, C. H., and Wentzel, T. J. (1990) *J. Phys. Chem. 94*, 4230−4235.
31. Kaufman, V., and Avnir, D. (1986) *Langmuir 2*, 717.
32. Pilch, D. S., and Shafer, R. H. (1993) *J. Am. Chem. Soc. 115*, 2565−2571.
33. Dagneaux, C., Liquier, J., Scaria, P. V., Shafer, R. H., and Taillandier, E. (1994) *Structural Biology: The State of the Art* (Sarma R. H., and Sarma M. H., Eds) Adenine Press, Guilderland, NY.
34. Scaria, P. V., Shire, S. J., and Shafer, R. H. (1992) *Proc. Natl. Acad. Sci. U.S.A. 89*, 10336−10340.
35. Scaria, A., Sugiura, S., Torigoe, H., and Shindo, H. (1993) *J. Biomol. Struct. Dyn. 11*, 245−252.
36. Scaria, P. V., and Shafer, R. H. (1996) *Biochemistry 35*, 10985−10994.
37. Keniry, M. A., Strahan, G. D., Owen, E. A., and Shafer, R. H. (1995) *Eur. J. Biochem. 233*, 631−643.
38. Svinarchuk, F., Monnot, M., Merle, A., Malvy, C., and Fermandjian, S. (1995) *Nucleic Acids Res. 23*, 3831−3836.
39. Svinarchuk, F, Paoletti, J., and Malvy, C. (1995) *J. Biol. Chem. 270*, 14068−14071.
40. Svinarchuk, F., Debin, A., Bertrand, J.-R., and Malvy, C. (1996) *Nucleic Acids Res. 24*, 295−302.
41. He, Y., Scaria, P. V., and Shafer, R. H. (1997) *Biopolymers 41*, 431−441.
42. IUPAC Commission on Photochemistry (1986) *EPA Newsl.* 21−29.
43. Koenig, P., Reines, S. A., and Cantor, C. R. (1977) *Biopolymers 16*, 2231−2242.
44. Dong, D. C., and Winnie, M. A. (1982) *Photochem. Photobiol. 35*, 17−21.
45. Tesler, J., Cruickshank, K. A., Morrison, I. E., Netzel, T. L., and Chan, K. (1989) *J. Am. Chem. Soc. 111*, 7226−7232.
46. Yamana, K., Grokota, T., Ozaki, H., Nakano, H., Sangen, O., and Shimidzu, T. (1992) *Nucleosides Nucleotides 11*, 383−390.
47. Kierzek, R., Li, Y., Turner, D. H., and Bevilacqua, P. (1993) *J. Am. Chem. Soc. 115*, 4985−4992.
48. Noonberg, S., François, J. C., Garestier, T., and Hélène, C. (1995) *Nucleic Acids Res. 23*,1956−1963.

49. Olivas, W. M., and Maher, J. L., III (1995) *Biochemistry 34*, 278−284.
50. Olivas, W. M., and Maher, J. L., III (1995) *Nucleic Acids Res. 23*, 1936−1941.
51. Maher, L. J., III, Dervan, P. B., and Wold, B. J. (1990) *Biochemistry 29*, 8820−8826.
52. Rougée M., Mergny, J. L., Barcelo, F., Giovannangeli, C., Garestier, T., and Hélène, C. (1992) *Biochemistry 31*, 9269−9278.
53. Xodo, L. E. (1995) *Eur. J. Biochem. 228*, 918−926.
54. Fox, K. R. (1995) *FEBS Lett. 357*, 312−316.
55. Ouali, M., Letellier, R., and Taillandier, E. (1996) *J. Mol. Struct 377*, 57−74.
56. Rao, B. J., Dutreix, M., and Radding, C. M. (1991) *Proc. Natl. Acad. Sci. U.S.A. 88*, 2984−2988.
57. Rao, B. J., and Radding, C. M. (1993) *Proc. Natl. Acad. Sci. U.S.A. 90*, 6646−6650.
58. Rao, B. J., and Radding, C. M. (1994) *Proc. Natl. Acad. Sci. U.S.A. 91*, 6161−6165.
59. Rooney S. M., and Moore, P. D. (1995) *Proc. Natl. Acad. Sci. U.S.A. 92*, 2141−2144.
60. Baliga, R., Singleton, J. W., and Dervan, P. B. (1995) *Proc. Natl. Acad. Sci. U.S.A. 92*, 10393−10397.

BI971710T